JOURNAL OF OPTOELECTRONICS AND ADVANCED MATERIALS Vol. 9, No. 4, April 2007, p. 1082 - 1086

Transient simulations of a rapid thermal processing apparatus

P.-O. LOGERAIS*, D. CHAPRON, A. BOUTEVILLE
LPMI, ENSAM, Angers, France
Annealsys, Montpellier, France

RTP (Rapid Thermal Processing) is a wide-spread technology to manufacture advanced semiconductors. It is used for oxidation, annealing, silicide formation and chemical vapour deposition. Numerical simulation is an essential step in order to have a better understanding of the Rapid Thermal Process. A preliminary work showed the influence of the quartz window on the wafer temperature profile. In the present study, a RTP reactor is modelled in two dimensions in order to analyse the wafer temperature evolution for a constant lamp heating power. Transient-state numerical simulations are then carried out, in which the radiative heat transfer equation is solved with the Monte-Carlo method. First, the general evolution of the wafer temperature is described. It can be subdivided into three different phases: a rapid increase, a slower one and the stabilisation. In the second part, the evolution of the centre to edge difference of temperature is analysed. An inversion of the wafer temperature profile occurs at the beginning of the heating and the maximal centre to edge difference of temperature is obtained when the steady-state has been reached. In both the parts, the corresponding evolution of the quartz window temperature is presented. A correlation between the wafer temperature evolution and the quartz window one is shown.

(Received November 2, 2006; accepted February 28, 2007)

Keywords: RTP, Numerical simulation, Wafer temperature uniformity, Quartz window, Rapid thermal processing

1. Introduction

Rapid Thermal Processes (RTP) are widely used in the microelectronics industry to manufacture advanced semiconductors. The processes are of different types, such as oxidation (RTO), annealing (RTA), silicide formation and chemical vapour deposition (RTCVD). Dimension shrinkage of the produced devices makes stringent demand on the knowledge of the thermal processing for the wafers. In order to obtain good quality thin films, the wafer surface temperature distribution must be uniform [1,2]. Consequently, the wafer temperature control and the thermal gradient reduction have become the main challenge [3,4]. In the recent years, simulation namely by using the computational fluid dynamics method (CFD), has appeared as a remarkable tool which puts into light the thermal and flow phenomena involved in the above mentioned processes [5,6].

In RTP reactors, a single wafer is loaded into a cold wall chamber. The wafer surface is then rapidly heated up by infrared lamps through a quartz window. A preliminary work showed that the quartz window has an influence on the wafer temperature profile [7]. It was shown that the substitution of the quartz window by nitrogen leads to a reduction of the wafer centre to edge difference of temperature (ctedt) for the steady-state calculations. The transient simulations revealed that the presence of the quartz window increases the steady state reaching duration.

In the present study, a commercial RTP reactor, the AS One 150 machine developed by AnnealSys (Montpellier) [8] is modelled in two dimensions. CFD simulations are performed to analyse both the wafer and the quartz window temperature evolution for a constant lamp heating power, which means without any process optimisation. Transient-state numerical simulations are carried out until the steady-state is reached. In order to solve the radiative heat transfer equation, the Monte-Carlo method is considered. First, a description of the RTP apparatus model is provided. In the second part, the general evolution of both the wafer and the quartz window temperature is presented. The centre to edge difference of temperature (ctedt) is described as well for both. The third part consists in analysing the different evolutions obtained.

2. Experimental and modelling

The 2D geometry model of the AS One 150 machine is provided by

Fig. 1. The heating system consists of a bank of eighteen infrared halogen lamps emitting with a tungsten filament. The lamp electrical power input is the same for all the lamps. The wafer is a 150 mm diameter silicon substrate and it is placed on quartz pins in the reaction chamber. It is heated by the radiative heat of the lamps through the quartz window, which is the upper reactor wall. To maintain the reaction chamber pressure low, a pumping system is used. Except for the quartz window, all the reaction chamber walls are stainless steel to reflect the rays emitted by the lamps on the wafer. They are cooled by a water circulation to avoid particule generation.

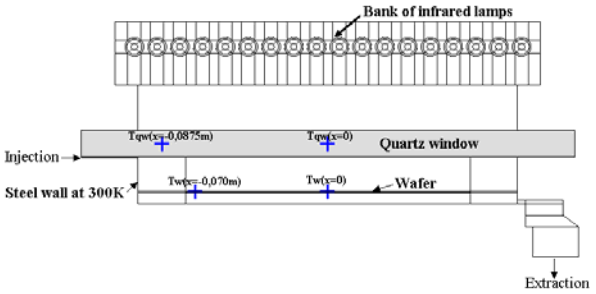

Fig. 1. The 2D AS One 150 machine geometry.

The commercial computational fluid dynamics software CFD'ACE is used to perform the calculations of heat and mass transfer [9]. The differential equations describing the conservation of mass and energy transport are solved using the finite volume method [10,11]. The differential equations are integrated over each control volume of the geometry domain. The generalized form of the conservation equation is given by expression (1). It is composed of four terms which respectively stand for the transient term, the convective term, the diffusion term and the source term.

$$\frac{\partial(\rho\phi)}{\partial t} + \nabla \cdot \left(\rho \vec{\nabla}\phi\right) = \nabla \cdot \left(\Gamma \nabla \phi\right) + S_{\phi} \qquad (1)$$

ρ is the density, t is the time, ϕ is the general flow variable, $\vec{V}$ is the velocity and Γ is the diffusion coefficient.

The Monte-Carlo method is used to solve the radiative heat transfer equation [12]. Its principle is as follows. The rays are grouped in photon bundles. The tracing of the photon bundles is done through the domain by accounting for the various events occurring within each control volume. Absorption, emission and scattering are the three possible events and the calculation of their coefficients is based on the optical index values of each material surface. Also, for each surface, Kirchhoff's law given by expression (2) is considered [13]. The total hemispherical emissivity $\varepsilon_{\theta,\lambda}$ is equal to the total hemispherical absorptivity $\alpha_{\theta,\lambda}$ for all spectral conditions:

$$\alpha_{\theta,\lambda} = \varepsilon_{\theta,\lambda}. \qquad (2)$$

The rays are emitted from a surface and traced until they are absorbed by the same surface or any other one. The tracing of the bundles also requires to statistically randomise the sample of photons from their points of emission to their points of absorption [14].

Calculations are performed in transient-sate. The implicit Euler method, which ensures unconditional numerical stability, is considered in the model [15].

In the model, the temperatures are taken in four places Fig. 1): one at the wafer centre $T_w(x=0)$, one at 5 mm from the wafer edge $T_w(x=-0,070m)$, one at the quartz window centre T_{qw} $(x=0)$ and one at a position close to the quartz window edge T_{qw} $(x=-0,0875m)$. Then, the centre to edge difference of temperature for the wafer $ctedt_w$ and the quartz window $ctedt_{qw}$ are expressed by (3) and (4):

$$ctedt_w = T_w(x=0) - T_w(x=-0,070m) \qquad (3)$$

$$ctedt_{qw} = T_{qw}\ (x=0) - T_{qw}\ (x=-0,0875m). \qquad (4)$$

3. Results

In order to obtain the temperature evolution of the wafer and the quartz window, simulations are carried out for three constant lamp heating power: a low one corresponding to a filament temperature of 1473 K, an average one (1773K) and a high one (2073K).

3.1 General evolution of the wafer and the quartz window temperature

Fig. 2 shows the temperature evolution at the wafer centre $T_w(x=0)$ and at the quartz window centre T_{qw} $(x=0)$ for the average heating power corresponding to the 1773K filament temperature. Similar shaped results are obtained for the whole wafer surface and for the quartz window. The shape stays the same for the low and the high heating power. The temperature evolutions in all the cases can be subdivided into three phases. The durations of the phases are respectively Δt_1, Δt_2 and Δt_3.

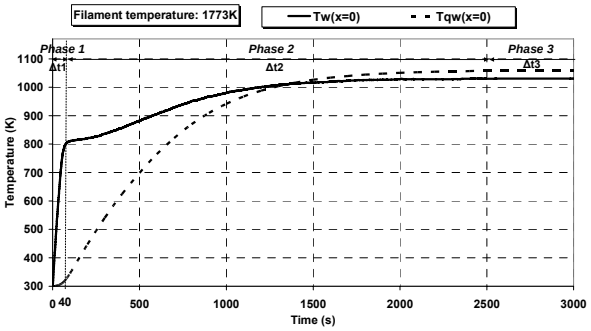

Fig. 2. Evolution of the centre wafer and quartz window temperature.

In the first phase, the wafer temperature increases rapidly in a linear way. In the second one, there is a step followed by another temperature increase which is slower than in phase 1. The increase becomes even slower once the wafer temperature is equal to the quartz window one. The third phase corresponds to the stabilisation of the wafer temperature.

The quartz window stays at initial temperature during the first phase. Then, its temperature increases during the second one. The increase is also slower once the quartz window temperature is equal to the wafer one. In the third phase, there is the temperature stabilisation as well.

The duration Δt_1 of the first phase is shorter when the heating power is higher, as shown in Fig. 3. The duration to reach steady-state Δt_2 is around 2500s for all the powers considered. Since steady-state is reached in the third phase, the Δt_3 duration is infinite.

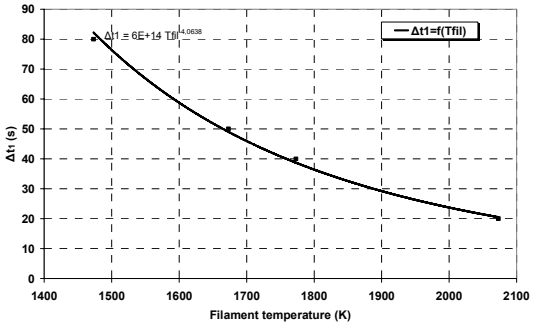

Fig. 3. Evolution of the duration Δt_1 in function of the heating power.

3.2 Evolution of the wafer and the quartz window ctedt

For the same heating powers, the wafer cdedt is calculated. The $ctedt_w$ evolution for the filament temperature of 1773K is given by Fig. 4. It can still be observed three phases with the same durations Δt_1, Δt_2 and Δt_3.

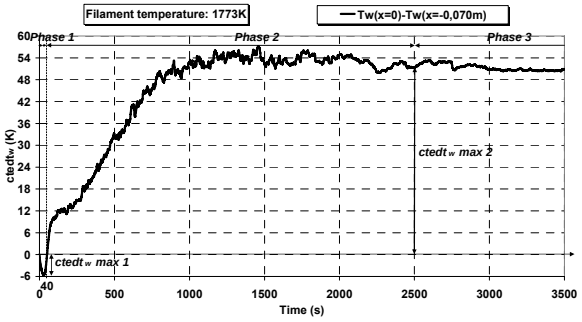

Fig. 4. Evolution of the wafer ctedt.

In the first phase, the $ctedt_w$ is negative that means the wafer temperature is higher at its edge. However, there is a strong decrease followed by an important increase. The difference between the minimal temperature and the x axis is called $ctedt_w$ *max 1*. It is more important when the lamp heating power is higher, as shown in Fig. 5. During the transition to the second phase, an inversion of the wafer temperature profile occurs. Fig. 6 illustrates this inversion. In the second phase, the wafer temperature profile becomes higher at the wafer centre. First, there is a very fast linear increase of $ctedt_w$, followed by a step and another increase. When the wafer and the quartz window temperatures become close to each other (at 1000s in the considered example), the $ctedt_w$ stabilises at its maximal value called $ctedt_w$ *max 2*. The latter value is also more important when the lamp heating power is higher (Fig. 5).

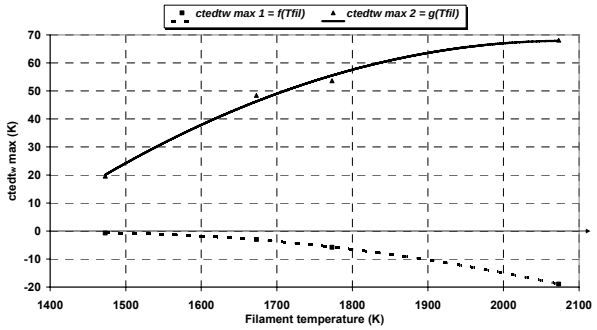

Fig. 5. Wafer $ctedt_w$ maximum differences versus heating power.

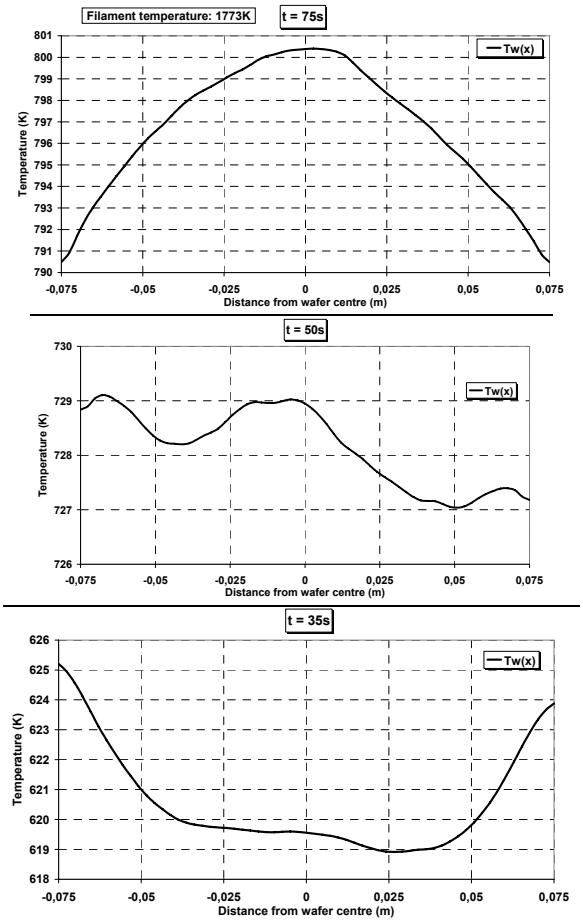

Fig. 6. Wafer temperature profile at different time.

The ctedt evolution is also obtained for the quartz window for the three same lamp powers. The division into three phases is also effective with the same durations. Fig. 7 gives the $ctedt_{qw}$ evolution considering the same 1773K filament temperature. $Ctedt_{qw}$ is close to zero in the first phase. But, in the second phase, there is an increase, which becomes slower once the quartz window temperature is close to the wafer one. The third phase corresponds to the stabilisation. Like the wafer, the ctedt is maximal in that phase.

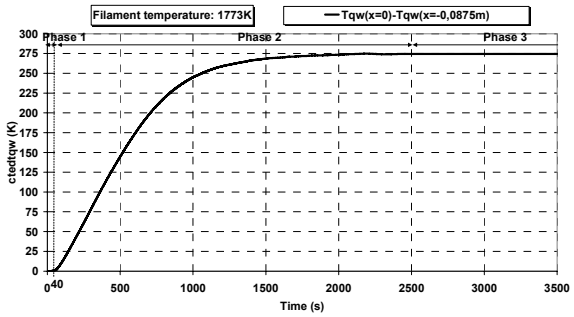

Fig. 7. Evolution of the quartz window ctedt$_{qw}$.

4. Discussion

4.1 General evolution of the wafer and quartz window temperature

As the infrared lamp emission is around 1µm in wavelength, the fast wafer temperature increase in the first phase is due to the wafer absorptivity evolution with the temperature (

Fig. *8*). The wafer absorptivity becomes more important above 1 µm when the temperature is higher. The quartz window absorbs the radiative part between 2.6 and 2.9 µm and beyond 3.6 µm as shown in

Fig. 9.

In phase 1, the quartz window stays at initial temperature because the wafer emission is low at the low temperatures of the beginning of the heating.

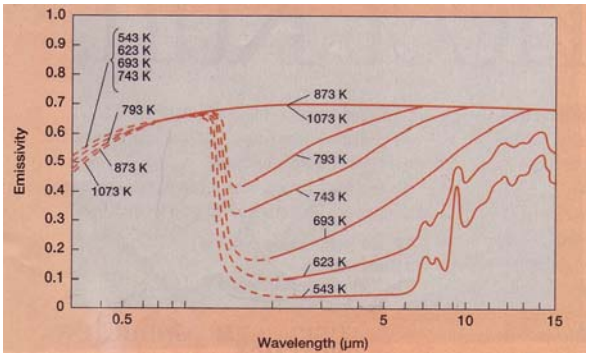

Fig. 8. Spectral emissivity of the silicon substrate [16].

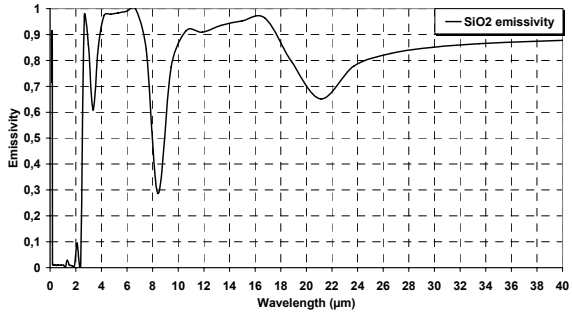

Fig. 9. Spectral emissivity of the quartz window [17].

In the second phase, for higher temperatures, the wafer emits with a coefficient getting closer to 0.7 in all the spectra

Fig. *8*). Thus, the quartz window absorbs the radiation emitted by the wafer explaining why its temperature increases. But, the radiation absorbed by the quartz window is also reemitted towards the wafer and contributes to the wafer temperature increase. So, there is a mutual heating by absorption and emission between the wafer and the quart window. Simulations confirm that in the absence of the quartz window, the steady-state is reached for the second phase [7].

When the temperatures of both the wafer and the quartz window are close to each other, the temperature increase becomes slower because there is a balance between the heat fluxes emitted and absorbed. It also means that steady-state is almost reached. The latter is reached in the third phase when all the heat fluxes are fully stabilised in the whole reactor.

4.2 Evolution of the wafer and the quartz window ctedt

In the first phase, the wafer temperature is higher at its edge than at its centre because the predominant effect is ray reflection on the reactor walls. The difference *ctedt$_w$ max 1* becomes more important when the lamp heating power is higher because the reflected rays are more numerous. A solution to reduce the *ctedt$_w$* at the beginning of the heating consists in putting a non-reflecting coating on the reaction chamber bottom, but unfortunately the response is slower [18].

The inversion of the wafer temperature profile occurring at the transition to the second phase is initiated when the *ctedt$_w$* starts its quick increase at the end of phase 1. The profile inversion is the combination of three effects. First, there is a conductive heat flux from the wafer edge to its centre. Secondly, when the wafer reaches elevated temperature, its emission towards the reactor cooled walls becomes higher than its emission towards the warm quartz window. Finally, the quartz window temperature is higher at its centre. So the heat flux from the quartz window towards the wafer is higher at the wafer centre compared to its edge. After the inversion, the quartz window c*tedt$_{qw}$* increases in phase 2 and so does the wafer c*tedt$_w$*.

When the steady state is reached in the third phase, the quartz window thermal gradient is at its highest value. The same goes for the wafer ctedt which is at the value *ctedt$_w$ max 2*. The *ctedt$_w$ max 2* value is more important when the lamp heating power is higher because the quartz window thermal gradient is also higher.

In order to improve the wafer temperature uniformity, reduction of the quartz window thermal gradient is the challenge. Consequently, double quartz window with oil or water circulation [19], cooling with a stream of air [20],

or with a showerhead [21] are solutions which have been studied or used.

5. Conclusion

The present study gives a better understanding of the temperature evolution in a RTP process. For that purpose, 2D transient simulations of a commercial apparatus have been analysed for a constant heating power. The wafer and the quartz window temperature evolutions have been followed.

The general temperature evolution can be subdivided into three different phases. For the wafer, there is a rapid increase, a slower one and the stabilisation. For the quartz window, a stay at initial temperature, followed by an increase and the stabilisation are the three phases. The absorption and emission properties of both the wafer and the quartz window explain the correlation between their temperature evolutions.

Furthermore, the centre to edge difference of temperature is analysed for the three phases. At the beginning of the heating, the wafer temperature is higher at its edge because of the dominant influence of ray reflection on the reactor walls. An inversion of the wafer temperature profile has been put into light during the transition between the first phase and the second one. In the second and third phase, the wafer non uniformity is correlated to the quartz window centre to edge difference of temperature. The difference is maximal when the steady-state is reached. Also, an increase of the thermal gradients is put into evidence when the heating power is higher.

All in all, to optimize the wafer temperature uniformity in RTP equipments, thermal gradients have to be reduced for the quartz window. With this aim, simulation studies are in progress.

References

[1] T. Fukada, S. Y. Woo, 12th IEEE International Conference on Advanced Thermal Processing of Semiconductors, RTP 2004, 129-134 (2004).

[2] A. Theodoropoulou, R. A. Adomaitis, E. Zafiriou, IEEE Transactions on Semiconductor Manufacturing, **11**(1), 85-98 (1998).

[3] M. Y. Ha, K. H. Lee, M. G. Bae, J. R. Cho, H. S. Lee, J. H. Choi, International Journal of Heat and Mass Transfer, **45**(11), 2303 (2002).

[4] J. L. Ebert, D. De Roover, L. L Porter II, V. A. Lisiwicz, S. Ghosal, R. L. Kosut, A. Emami-Naeini, Proceedings of the American Control Conference, **5**, 3910-3921(2004).

[5] C. Tanasa, J. Ranish, A. Hunter, S. Ramamurthy, R. Jallepally, B. Ramachandran, C. Lai, A. Tjandra , N. Tam, 12th IEEE International Conference on Advanced Thermal Processing of Semiconductors, RTP 2004, 181-184(2004).

[6] J. Liu, Y.S. Chen, Numerical Heat Transfer, Part A: Applications, **38**(2), 129-152 (2000).

[7] P. O. Logerais, M. Girtan, A. Bouteville, J. Optoelectron. Adv. Mater. **8**(1), 139 (2006).

[8] *AS One 150* is an AnnealSys product, Montpellier, France (www.annealsys.com).

[9] CFD'ACE software is an ESI group product, Huntsville, USA (www.esi-group.com).

[10] CFD Research Corporation, CFD'ACE (U) User Manual, Version 2004, (2004).

[11] H.V. Versteeg and W. Malalasekera, An introduction to computational fluid dynamics, The finite volume method, Longman, London (1995).

[12] CFD Research Corporation, CFD'ACE (U) Module Manual, Version 2004, (2004).

[13] F. Incropera, D.P. Dewitt, Fundamentals of Heat and Mass Transfer, John Wiley and Sons, New York (1996).

[14] M. F. Modest, Radiative Heat Transfer, McGraw-Hill International Editions (1993).

[15] S. V. Patankar, Numerical Heat Transfer and Fluid Flow, Hemisphere Publishing Corporation, McGraw-Hill Book Company, New York (1980).

[16] T. Sato, Japanese Journal of Applied Physics **6**(3), 339 (1967).

[17] E. D. Palik, Handbook of Optical Constants of Solids, Academic Press, Orlando (1998).

[18] L. Plévert, Cristallisation par recuit rapide du silicium amorphe sur verre, thèse doctorat, Université Rennes I (1995).

[19] A. Slaoui, S. Bourdais, G. Beaucarne, J. Poortmans, S. Reber, Solar Energy Materials and Solar Cells, **71**(2), 245 (2002).

[20] E. Dassau, B. Grosman, D. R. Lewin, Computers and Chemical Engineering, **30**(4), 686-697 (2006).

[21] C. P. Yin, C. C. Hsiao, T. F. Lin, Journal of Crystal Growth, **217,** 201 (2000).

*Corresponding author: logerais@angers.ensam.fr